Eur. Phys. J. A **15**, 299–302 (2002)
DOI 10.1140/epja/i2002-10082-0

THE EUROPEAN PHYSICAL JOURNAL A

Short Note

Rotational alignment of the $h_{11/2}$ band in ^{157}Dy

T. Hayakawa[1,a], Y. Toh[1], M. Oshima[1], M. Matsuda[1], Y. Hatsukawa[1], J. Katakura[1], H. Iimura[1], T. Shizuma[1], S. Mitarai[2], M. Sugawara[3], H. Kusakari[4], and Y.H. Zhang[5]

[1] Japan Atomic Energy Research Institute, Tokai, Ibaraki 319-1195, Japan
[2] Kyushu University, Hakozaki, Fukuoka 812-8581, Japan
[3] Chiba Institute of Technology, Narashino, Chiba 275-8588, Japan
[4] Chiba University, Inage-ku, Chiba 263-8522, Japan
[5] Institute of Modern Physics, Chinese Academy of Science, Lanzhou 730000, PRC

Received: 22 August 2002 / Revised version: 24 September 2002 /
Published online: 19 November 2002 –
Communicated by W. Henning

Abstract. High-spin states of ^{157}Dy were investigated using in-beam γ-ray spectroscopy techniques with a ^{150}Nd(^{12}C, 5n) reaction. Three rotational bands with the $h_{9/2}$, $i_{13/2}$ and $h_{11/2}$ configurations were observed up to $(43/2^-)$, $53/2^+$ and $45/2^-$, respectively. Interband $M1$ transitions in the $h_{11/2}$ (high-Ω) band were also measured up to the highest-spin state. The high-spin states were well reproduced by calculations using the tilted-axis-cranking model (TAC). The $B(M1)/B(E2)$ ratio, Routhian and the tilted angle of the angular-momentum vector are found to be in good agreement with the result of the TAC calculation.

PACS. 23.20.Lv Gamma transitions and level energies – 27.70.+q $150 \leq A \leq 189$ – 21.60.Ev Collective models

Nuclei in the mass $A \sim 150$ region have been characterized by the interplay of collective motions and single-particle excitations [1]. Nuclear deformations in this mass region show a gradual transition from a spherical shape in a closed shell to a prolate deformation with increased neutron number. The interaction between the single-particle orbits and the collective motion can be clarified through a study of odd-mass nuclei. Nuclei heavier than $N = 90$ in this mass region, which exhibit a band structure with high quadrupole deformation, were studied by in-beam γ-ray spectroscopy, for example, see refs. [2–5]. The nucleus ^{157}Dy is an $N = 91$ isotone having a typical rotational structure. The last neutron in ^{157}Dy can occupy various single-particle orbitals near the Fermi surface. Assuming $\beta_2 = 0.25$–0.28 as a deformation parameter, the substantial Nilsson orbits for neutrons are $h_{11/2}$ ($[505]\frac{11}{2}^-$), $i_{13/2}$ ($[651]\frac{3}{2}^+$) and $h_{9/2}$ ($[521]\frac{3}{2}^-$), each of which has a different effect on rotational bands depending on the Ω value; the $[505]\frac{11}{2}^-$ single-particle configuration with high-Ω quantum number leads to a strong-coupling scheme, while the $[651]\frac{3}{2}^+$ and $[521]\frac{3}{2}^-$ configurations with low-Ω leads to a weak-coupling scheme. Furthermore, nuclei in

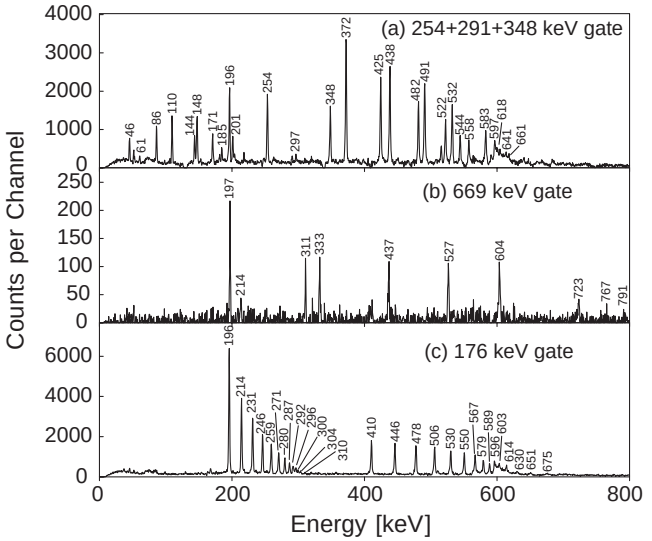

Fig. 1. Typical gated spectra in ^{157}Dy. (a) A sum spectrum gated by the 254, 291 and 348 keV γ-ray in Band 1. (b) A spectrum gated by the 669 keV γ-ray in Band 2. (c) A spectrum gated by the 176 keV γ-ray in Band 3.

[a] e-mail: hayakawa@jball4.tokai.jaeri.go.jp

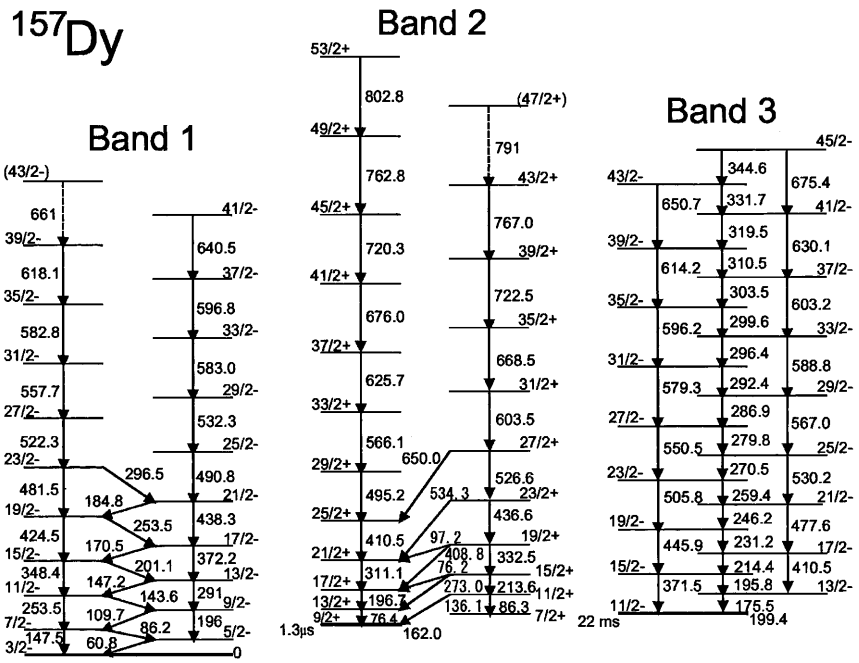

Fig. 2. Partial level scheme of ^{157}Dy constructed from the current experiment. Three typical rotational bands consisted of $E2$ cascade and interband $M1$ transitions were observed. The half-life and excitation energy of the band head of Bands 2 and 3 are taken from ref. [13].

$N = 91, 93$ isotones have the following feature: the excitation energy of the ground-state band with the $h_{9/2}$ configuration increases quickly with increasing angular momentum, whereas the $i_{13/2}$ band becomes to be the yrast state above several hundred keV. The enhanced $E1$ transitions from the $h_{9/2}$ band to the $i_{13/2}$ band in $N = 93$ isotones were observed in high-spin states [3], but not in $N = 91$ isotopes [5–7]. In our previous work, high-spin states in ^{155}Gd ($N = 91$) were studied through an in-beam γ-ray spectroscopy [5]. The rotational bands with the $i_{13/2}$ and $h_{11/2}$ configurations were observed. Furthermore, the $M1$ transitions in the high-Ω $h_{11/2}$ band were also measured up to $(37/2)^-$. The $B(M1)/B(E2)$ ratios, the tilted angle of the angular-momentum vector in the intrinsic frame and Routhian were calculated using the tilted-axis-cranking (TAC) model. The TAC calculation reasonably reproduced both the $B(M1)/B(E2)$ ratio and tilted angle in the $h_{11/2}$ band simultaneously. High-spin states of the ^{157}Dy nucleus, which is an isotone of the ^{155}Gd, were studied using in-beam γ-ray spectroscopy [6, 8–11]. Although the favoured band of the $i_{13/2}$ configuration in ^{157}Dy was measured up to $81/2^+$ in a previous experiment [6], while the $h_{11/2}$ band with high-Ω and the $h_{9/2}$ band have only been measured up to $25/2^-$ and $21/2^-$, respectively [8]. In order to study the rotational collective motion and the effect of the tilting degrees of freedom of the angular-momentum vector in the high-Ω band in ^{157}Dy, an in-beam γ-ray spectroscopy using a ^{150}Nd(^{12}C, 5n)^{157}Dy reaction was carried out.

The nucleus ^{157}Dy was produced with the ^{150}Nd(^{12}C, 5n)^{157}Dy reaction using the ^{12}C beam with a 65 MeV energy provided by the tandem accelerator at the Japan Atomic Energy Research Institute (JAERI). The target was a self-supporting ^{150}Nd metallic foil enriched to 96.1% with a thickness of 2 mg/cm^2. Gamma-rays from excited states populated by the reaction were detected with the GEMINI detector system [12] which is an array of 12 HPGe detectors with BGO Compton suppressors. The HPGe detectors were placed at angles of 32°, 58°, 90°, 122° and 148° with respect to the beam direction. The energy resolutions of HPGe detectors were 2.0–2.3 keV at 1.3 MeV and the typical efficiencies were about 40–70% relative to $3'' \times 3''$ NaI detector. The experimental data were recorded on magnetic tapes event by event when two or more HPGe detectors were responded. After this experiment, the double or higher fold γ-γ coincidence events were sorted to E_γ-E_γ matrices, and thereby approximate 2×10^8 γ-γ coincidence events were collected. The gated spectra were created from the 4096 channel $\times$ 4096 channel matrices. A level scheme was constructed from the coincidence relationship, intensity balance and DCO ratio. The relative intensities were derived from both the singles and gated spectra. The spin assignment was made from the DCO ratio of 32° and 90°. Assuming dipole transitions to be pure, the $B(M1)/B(E2)$ ratios of the $h_{11/2}$ band could be deduced from the relative intensities using the following relation:

$$\frac{B(M1: I \to I-1)}{B(E2: I \to I-2)}[\mu_N/\mathrm{eb}] = 0.697 \times \frac{E_\gamma^5(E2)[\mathrm{in\ MeV}]}{E_\gamma^3(M1)[\mathrm{in\ MeV}]} \times \frac{I_\gamma(M1)}{I_\gamma(E2)}\,. \quad (1)$$

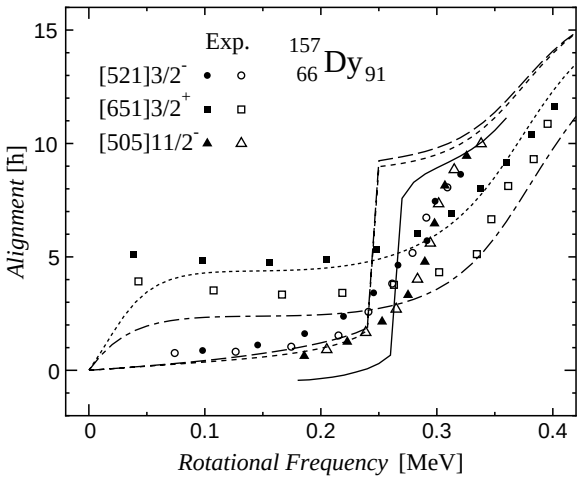

Fig. 3. Alignment of the three bands. Solid lines express the result by TAC calculation. A simple reference band with a constant moment of inertia $J_0 = 27.8$ for experimental data and $J_0 = 25.0$ for the calculation were used.

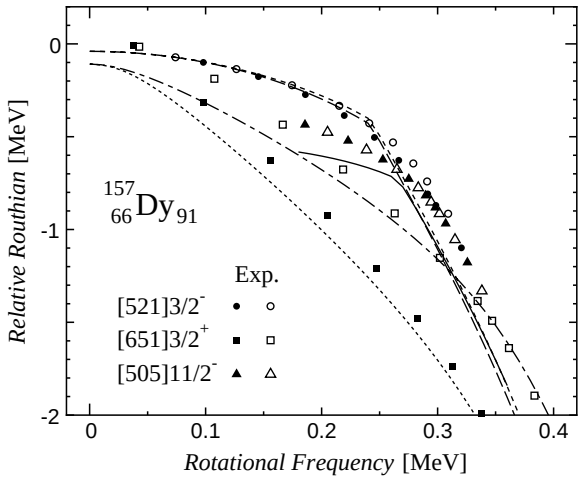

Fig. 4. Routhian of the three bands. Solid lines express the result by TAC calculation. A simple reference band with a constant moment of inertia $J_0 = 27.8$ for experimental data and $J_0 = 25.0$ for the calculation were used.

Figure 1 shows some gated spectra, in which typical rotational bands consisting of $E2$ cascades and interband $M1$ transitions are shown. Figure 2 shows the partial level scheme that was constructed from the γ-γ coincidence relationships and intensity balances. In previous experiments, three bands with the $h_{9/2}$ (Band 1), $i_{13/2}$ (Band 2) and $h_{11/2}$ (Band 3) configurations were observed up to $21/2^-$, $81/2^+$ and $25/2^-$, respectively. The γ-decays from the band heads of the $i_{13/2}$ and $h_{11/2}$ configurations were not observed, because of long half-lives of the band heads with 1.3 μs and 22 ms, respectively [13]. Band 1, which is the ground-state band, has two $E2$ cascades and $M1$ transitions in low-spin states. In the present experiment, Bands 1 and 3 were extended up to $(43/2^-)$ and $45/2^-$, respectively. Band 2 that is the yrast band in high-spin states shows large signature splitting, of which the interband $M1$ transitions were observed at the low-spin states. Although the favoured band of Band 2 was reported up to $81/2^+$, the highest state of the unfavoured band was only $31/2^+$ [14]. Four γ-rays were newly found at the top of the unfavored band. Band 3 consists of the $E2$ transitions and $M1$ transitions, both of which are extended up to the $45/2^-$ state. The small signature splitting in this band indicates the high-Ω configuration. In the ^{159}Dy nucleus, the $E1$ interband transitions from the $h_{9/2}$ band to the $i_{13/2}$ band were observed up to the $41/2^-$ state using a fusion-evaporation experiment [3], whereas the $E1$ interband transitions could not be observed in the current experiment.

Recently, it has been recognized that the effects of the degrees of freedom, which were defined by the angle between the angular-momentum vector and the inertia axes of deformation, were well explained by the tilted-axis-cranking (TAC) model [15–17]. In the case of a high-j quasi-particle coupled to a rotor, it was shown that the results of the particle-rotor model and the TAC approximation were very similar [16,18]. S.-I. Ohtsubo and Y.R. Shimizu have systematically studied high-spin states in the $N = 91, 93$ isotones in the light–rare-earth region using the TAC calculation [5,19]. The following result of the TAC calculation was taken from ref. [19]. In the TAC calculation, a deformation parameter has been an important factor to understand high-spin states. The deformation parameters $\epsilon_2 = 0.256$ and $\epsilon_4 = -0.0181$ ($\gamma = 0$) were used, which gave approximately the measured quadrupole moment [20]. The pairing gap parameters have also been important for the TAC calculation. The constant values of $\Delta_\nu = 0.821$ MeV and $\Delta_\pi = 0.988$ MeV were used, which reproduced the experimental data of the neighboring even-odd mass difference. Figure 3 shows the experimental and calculated alignments of the three bands. Figure 4 shows the TAC calculated Routhian in comparison with the observed ones. The difference between the calculation and experimental data in the $h_{11/2}$ band is observed in low rotational frequencies, while the degeneration of the $h_{11/2}$ band and the $h_{9/2}$ band in high frequencies is well reproduced. A most interesting observation in the present experiment is that the $B(M1)/B(E2)$ ratios were measured up to high-spin states for Band 3. As is shown in fig. 5 the $B(M1)/B(E2)$ ratios decrease with increasing angular momentum. This behavior is qualitatively understood by a formula of the strong-coupling limit of the rotor model [21,22]:

$$\frac{B(M1; I \to I-1)}{B(E2; I \to I-2)} = \frac{12}{5}\frac{(g_K - g_R)^2 K^2}{Q_0^2}\frac{\langle IK1K|I-1K\rangle^2}{\langle IK2K|I-2K\rangle^2} \approx \frac{16}{5}\frac{(g_K - g_R)^2 K^2}{Q_0^2}\frac{\sin^2\theta_{I-1/2}}{\sin^4\theta_{I-1}}, \quad (2)$$

with

$$\cos\theta_I \equiv \frac{K}{I+1/2}, \quad (3)$$

where g_K, g_R and Q_0 are the appropriate g-factors and the quadrupole moment for the band. The θ_I in the second line expresses the angle between the total angular momentum

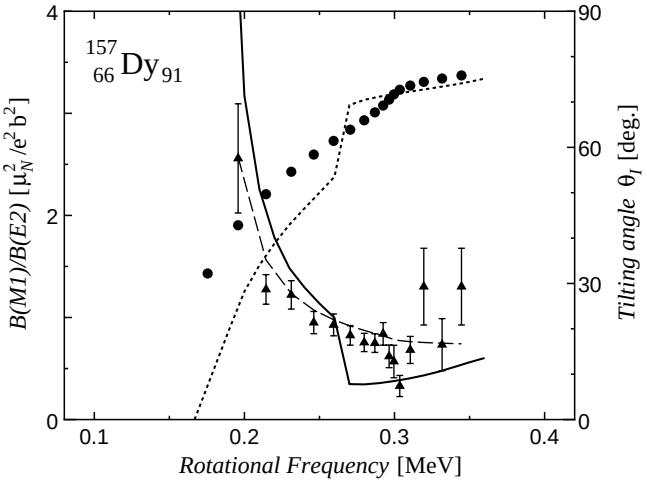

Fig. 5. The $B(E1)/B(E2)$ values and tilted angle of the rotational alignment. The solid line denotes the result of the TAC calculation. The dashed line denotes the result of the strong-coupling formula, where the parameter $[(g_K - g_R)K/Q_0]^2$ is adjusted to fit the data.

and the symmetry axis (z-axis) of the deformed potential, and the asymptotic expressions of the Clebsch-Gordan coefficient are used. As is clear in eq. (2) the ratio is quite sensitive to the geometry of the angular-momentum vector in the intrinsic frame. The results of the tilting angle and the $B(M1)/B(E2)$ ratio for Band 3 as functions of frequency are shown in fig. 5. The angle θ_I estimated by eq. (3) from the frequency and the angular momentum with fixed K value is also included. The $B(M1)/B(E2)$ ratio decreases with increasing the frequency, and the tilted angle has the opposite tendency. The experimental $B(M1)/B(E2)$ ratio and tilted angle were well reproduced by the TAC calculation. The effects of the alignment caused by the $i_{13/2}$ two quasi-particles were observed in both the experimental $B(M1)/B(E2)$ ratios and the Routhian at a rotational frequency 0.29–0.3 MeV, where the measured $B(M1)/B(E2)$ ratio dropped. The particle-rotor model cannot reproduce the alignment because of the limit of the macroscopic model. These effects were calculated through the TAC model, but the alignment effects of the $B(M1)/B(E2)$ and the Routhian appear at a frequency 0.27 MeV lower than the experimental result.

In summary, high-spin states of ^{157}Dy were investigated using the ^{150}Nd(^{12}C, 5n) reaction. Three rotational bands with the $h_{9/2}$, $i_{13/2}$ and $h_{11/2}$ configurations were observed up to $(43/2^-)$, $53/2^+$ and $45/2^-$, respectively. The interband $M1$ transitions in the $h_{11/2}$ band were also measured up to the highest-spin state, and the drop of the $B(M1)/B(E2)$ ratios caused by the alignment of two quasi-particles was observed in the $h_{11/2}$ band. The high-spin states were well reproduced by the calculation of the TAC model. The $B(M1)/B(E2)$ ratio, Routhian and the titled angle between the total angular momentum and the symmetry axis of the deformed potential in the $h_{11/2}$ band had a good agreement with the result of the TAC calculation. The effects of the alignment were also reproduced, but the calculated rotational frequency was lower than the one observed in experiment.

We thank the crew of the JAERI tandem accelerator for providing the heavy-ion beams and Prof. G. Sletten in NBI for providing the ^{150}Nd target. We also thank Dr. Shimizu and Dr. Ohtsubo for many discussions concerning the analysis of our experimental data.

References

1. W. Nazarewicz, M.A. Riley, J.D. Garrett, Nucl. Phys. A **512**, 61 (1990).
2. J. Simpson *et al.*, Eur. Phys. J. A **1**, 267 (1998).
3. M. Sugawara *et al.*, Nucl. Phys. A **699**, 450 (2002).
4. X. Liang *et al.*, Eur. Phys. J. A **10**, 41 (2001).
5. T. Hayakawa *et al.*, Nucl. Phys. A **657**, 3 (1999).
6. M.A. Riley *et al.*, Z. Phys. A **345**, 121 (1993).
7. J.Y. Huh *et al.*, Eur. Phys. J. A **7**, 11 (2000).
8. W. Klamra *et al.*, Nucl. Phys. A **199**, 81 (1973).
9. H. Beuscher *et al.*, Nucl. Phys. A **249**, 379 (1975).
10. S.A. Hjorth *et al.*, Z. Phys. A **283**, 287 (1977).
11. H. Emiling *et al.*, Nucl. Phys. A **419**, 187 (1984).
12. K. Furuno *et al.*, Nucl. Instrum. Methods Phys. Res. A **421**, 211 (1999).
13. R.B. Firestone *et al.*, *Table of Isotopes*, eighth edition (Wiley Interscience, 1998).
14. T. Hayakawa *et al.*, Eur. Phys. J. A **9**, 153 (2000).
15. S. Frauendorf, Nucl. Phys. A **557**, 259c (1993).
16. S. Frauendorf, J. Meng, Z. Phys. A **356**, 263 (1996).
17. S. Frauendorf, Z. Phys. A **358**, 163 (1997) .
18. S.-I. Ohtsubo, Y.R. Shimizu, Prog. Theor. Phys. **98**, 1099 (1997).
19. S.-I. Ohtsubo, Y.R. Shimizu, to be published in Nucl. Phys. A.
20. K.E.G. Löbner, M. Vetter, V. Hönig, Nucl. Data Tables A **7**, 495 (1970).
21. Å. Bohr, B.R. Mottelson, *Nuclear Structure*, Vol. **II** (Benjamin, New York, 1969).
22. T. Kutsarova *et al.*, Nucl. Phys. A **587**, 111 (1995).